

# Combination of different SAR modalities for geospatial intelligence applications in a harbor environment

Dirk C. Borghys <sup>a</sup>

Azzedine Bouaraba <sup>b</sup>

Christiaan Perneel <sup>c</sup>

<sup>a</sup>Royal Military Academy, Dept. CISS, Renaissancelaan 30 , Brussels, Belgium

<sup>b</sup>Ecole Militaire Polytechnique, BP17, Bordj-el-Bahri, Algiers, Algeria

<sup>c</sup>Royal Military Academy, Dept. of Math., Renaissancelaan 30 , Brussels, Belgium

## ABSTRACT

Since the launch of Terrasar-X, Radarsat 2 and the Cosmo-Skymed constellation, spaceborne SAR data with a high spatial resolution have become more readily available, allowing to monitor areas with a high level of human activity independent of weather circumstances. The current paper investigates the use of such data for geospatial intelligence applications in an harbor environment. The applications of interest are change detection and activity monitoring. For the analysis a set of more than twenty datasets from the three above mentioned satellite systems, acquired over a period of 30 days over the sea harbor of Zeebrugge in Belgium is available. Most datasets are high-resolution spotlight mode, but some scansar and full-polarimetric data have also been acquired. In the current paper HiRes spotlight data from the Cosmo-Skymed constellation are used for change detection and activity monitoring in the port.

**Keywords:** interferometric SAR, change detection, activity monitoring, harbor scene analysis

## 1. INTRODUCTION

Change detection using multi-temporal Synthetic Aperture Radar SAR is a very important application of remote sensing.<sup>1-3</sup> Because SAR data can be acquired independent of weather and sunlight conditions and because of the availability of high-temporal coverage offered by the different spaceborne SAR systems, satellite SAR data have become very attractive for the continuous monitoring of changes in areas with high activity. To identify changes using SAR data, different methods are commonly applied. Since SAR data contain amplitude and phase information, both parameters can be used as change indicators.<sup>2</sup> With the advent of high-resolution SAR images, Coherent Change Detection (CCD) applications where coherence between two SAR images is evaluated and analyzed to detect surface change, has received a lot of attention.<sup>4-6</sup> The currently available spatial resolution allows to detect detailed changes of human activity indicators, such as changes in the stacking of containers in a port<sup>7</sup> from spaceborne SAR data.

In the current paper information from interferometric coherence and intensity is combined for an application of activity monitoring in a commercial harbor. The presented work is part of a project on the use of space-borne SAR for the geospatial analysis of maritime environments. The area of interest in the harbor of Zeebrugge in Belgium. Zeebrugge is a maritime commercial port consisting of three parts: an outer port, an inner port and the seaport of Brugge. The area of interest in the presented work is focussed on the outer port which consists of a liquefied natural gas terminal, several container terminals, two roll-on/roll-off terminals for freight and passengers and berth for cruise ships and passenger ships.<sup>8</sup>

While CCD images allow photo-interpreters to detect and analyze changes, continuous monitoring requires a semi-automatic approach. Therefore the current paper proposes a method for semi-automatic detection and

---

Further author information: (Send correspondence to Dirk Borghys)  
Dirk Borghys: E-mail: Dirk.Borghys@elec.rma.ac.be, Telephone: +32 2 742 6660

characterization of changes. The method is applied to high-resolution (enhanced spotlight) interferometric SAR pairs from the COSMO-Skymed constellation acquired in a period of 30 days over the Port of Zeebrugge. The paper illustrates the benefit of applying a filter for improving both the coherence information (bias reduction) and intensity information (speckle reduction) for establishing a semi-automatic processing chain for change detection.

The paper is organized as follows. First an overview of the used dataset is presented (section 2). Section 3 describes the processing chain for the semi-automatic detection and characterization of changes. In section 4 ship detection is presented as an application of the change detection results.

## 2. OVERVIEW OF THE DATASET

A set of more than 20 images from the three SAR satellites was acquired over the sea harbor of Zeebrugge in Belgium in a period of 30 days. These data provide a high-temporal density for activity monitoring. In the current paper the concept of monitoring of human activity is illustrated based on a set of five high-resolution spotlight SAR data from the Cosmo-Skymed constellation. These five datasets were acquired using the same geometry, allowing InSAR processing. Table 2 presents the main characteristics of the data.

Acquisition dates	:	15jun11	16jun11	19jun11	1jul11	2jul11
Satellite Name	:	CSK-2	CSK-3	CSK-4	CSK-2	CSK-3
Acquisition time	:	18h06 UTC				
Pass	:	Descending				
Sensor Mode	:	Enhanced Spotlight				
Polarisation	:	HH				
Incidence Angle	:	27.8 °				
Azimuth resolution	:	1.08 m				
Range resolution	:	0.88 m				
Image size	:	5102 × 4829				

Table 1. Overview of the dataset used in this paper

## 3. DETECTION AND CHARACTERIZATION OF CHANGES USING COHERENCE AND INTENSITY CHARACTERISTICS

For the change detection a semi-supervised approach based on interferometric coherence and intensity characteristics was developed. The idea is that changes due to human activity should be characterized by a low coherence magnitude and a high intensity in at least one of the two images of an interferometric couple. The intention was to use a very simple processing chain that can easily be automated. Therefore the defined learning set is kept very limited and consists of only three classes. Figure 1 presents a schematic overview of the processing chain used for the detection and classification of changes. The various steps are explained in the following sections.

### 3.1 Definition of the learning set

The learning set used for the semi-supervised change detection consists of three classes: Unchanged land, Water and Changes on land. For each of the classes an area of approximately 3000 pixels was identified in the scene. For the two first classes the same location can be used in all images. For the last class, a region with changes in one of the the container terminal areas, was identified. This area differs slightly between the different interferometric couples. The learning set is used for determining thresholds for the semi-automatic change detection and characterisation.

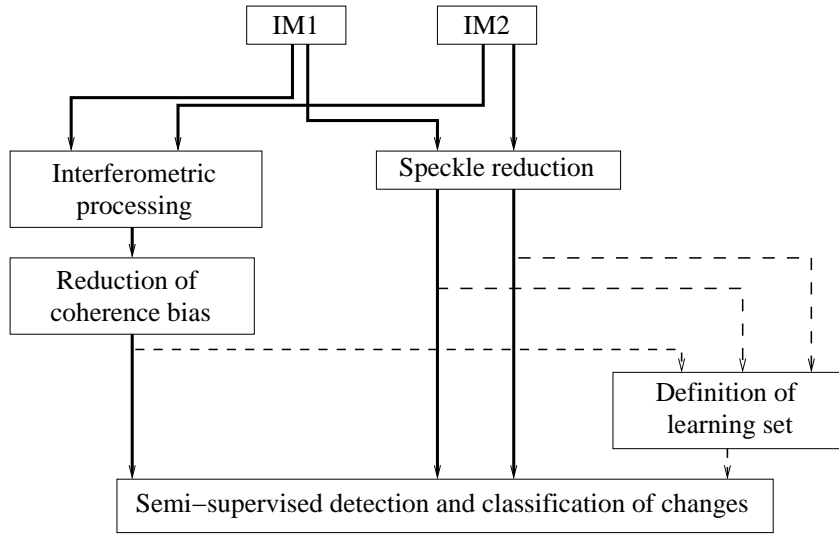


Figure 1. Schematic overview of the change detection processing

## 3.2 Coherence estimation and bias reduction

### 3.2.1 The interferometric couples

For the interferometric processing, the image of 15jun11 was used as master and the five others as slave images. A 3 by 3 multilooking was used for the interferometric processing. Table 3.2.1 presents an overview of the InSAR baseline characteristics.

Date	Time baseline	Normal Baseline	$2\pi$ ambiguity height	$2\pi$ ambiguity displacement
16 jun 11	1d	64.16 m	79.7 m	16 mm
19 jun 11	4d	22.7 m	231.9 m	16 mm
01 jul 11	16d	529.5 m	9.6 m	16 mm
02 jul 11	17d	425.9 m	12.0 m	16 mm

Table 2. Overview of the InSAR baseline characteristics

### 3.2.2 Interferometric SAR coherence

The sample complex interferometric coherence is defined as:

$$\gamma = \frac{\sum_{i=1}^N I_1(i) I_2^*(i)}{\sqrt{\sum_{i=1}^N |I_1(i)|^2} \sqrt{\sum_{i=1}^N |I_2(i)|^2}} \quad (1)$$

where  $I_1$  and  $I_2$  are the two images forming the interferometric couple,  $N$  is the size of the scanning rectangle used in the calculation. In the current experiment  $N = 9$ , which corresponds to a  $3 \times 3$  scanning window. The coherence can be expressed as the product of a number of dominant contributions:<sup>4</sup>

$$\gamma = \gamma_{SNR} \gamma_{base} \gamma_{scene} \gamma_{vol} \gamma_{proc} \quad (2)$$

where:

- $\gamma_{SNR}$  is determined by the relative backscatter signal to radar receiver noise ratio in the interferometric image pair.

- $\gamma_{base}$  quantifies the decorrelation that arises due to mismatch in the acquisition geometries between the two images.
- $\gamma_{vol}$  is the decorrelation that arises when the scattering occurs from a volume such as a vegetated area.
- $\gamma_{proc}$  is the decorrelation arising from mismatch between the coherent acquisition apertures and image-formation processing stages used to produce the two images.
- $\gamma_{scene}$  is the decorrelation in the scene over the repeat-pass time interval. This includes man- made scene changes but also environmental effects such as wind and rain.

Through a careful design of the repeat-pass imaging geometry and appropriate interferometric processing steps, it is possible to achieve  $\gamma_{SNR}\gamma_{base}\gamma_{proc} = 1$ . In this case, the coherence of the scene image will reflect the underlying true scene coherence and the coherence loss due to volume scatterers.

### 3.2.3 Coherence bias and bias reduction

The sample complex coherence in eq. 1 is a biased estimator of the coherence.<sup>9</sup> The bias is more important for low values of the coherence. This leads to detection errors (mainly false detections). The effect of the bias is inversely proportional to the size of the scanning window in which the coherence is calculated.<sup>9</sup> Increasing the size of the scanning window would thus reduce the bias. However, in our case, small changes can be of interest and averaging over large areas will deteriorate the detection of small changes. An alternative is to spatially average the coherence image. Two methods can be applied:

- Averaging of the coherence magnitude:  $\gamma_M(x, y) = \frac{1}{M} \sum_{i=1}^M |\gamma(i)|$ .  $M$  is the dimension of the averaging window.
- Averaging of the complex coherence:  $\gamma_{CM}(x, y) = \frac{1}{M} \left| \sum_{i=1}^M \gamma(i) \right|$

In Ref. 10 it is shown that applying a two-level coherence estimation and using the complex coherence instead of the coherence magnitude, significantly improves the detection of coherent changes. Fig. 2 shows the histograms of the coherence magnitude  $|\gamma|$  for the three objects of the learning set after three types of processing: the magnitude of the original coherence, estimated on a  $3 \times 3$  window (Orig), the coherence magnitude after a  $3 \times 3$  spatial averaging of  $|\gamma|$  (denoted M3x3 in the figure) and the magnitude of the  $3 \times 3$  spatially averaged complex coherence (CM3x3). The figure shows that the spatial averaging indeed improves the separability between the area of "no change" at one hand and the water and "container changes" areas on the other hand. The figure also shows that water surfaces would be classified as areas of changes when only coherence information is used. Fig. 3 shows the receiver-operator characteristic (RoC) curves for the three approaches for detecting the changes in the container area with respect to the area of no change. The RoC curves are based on the learning set and constructed using the coherence images only. It is clear that the spatial averaging improves results of the change detection based on coherence and that the averaging of the complex coherence gives slightly better results than the averaging of the coherence magnitude. In Ref. 10 it was shown that the difference between the two averaging methods is only significant for small averaging windows.

### 3.3 Speckle reduction on intensity data

For the detection of human activity the coherence information needs to be combined with intensity data. Fig. 4 (left) shows a color composite of the original coherence magnitude and the logarithm of the intensity of the two images forming the interferometric pair.. We suppose that man-made objects present a high radar return. Human activity is thus characterized by a low coherence and a high intensity in at least one of the two images (i.e. the areas that show a combination of green and blue in fig.4).

However any decision based on amplitude is hampered by the presence of speckle. Speckle leads to an increase of false alarms. Therefore a speckle reduction is performed prior to the change detection. In this paper a  $5 \times 5$  Lee filter<sup>11</sup> was applied, but we will investigate other speckle reduction methods in future. In fig. 5 the histograms of the three training areas are shown before and after speckle reduction. The figure shows that the area of "container changes" is better distinguishable from the two other areas after speckle reduction.

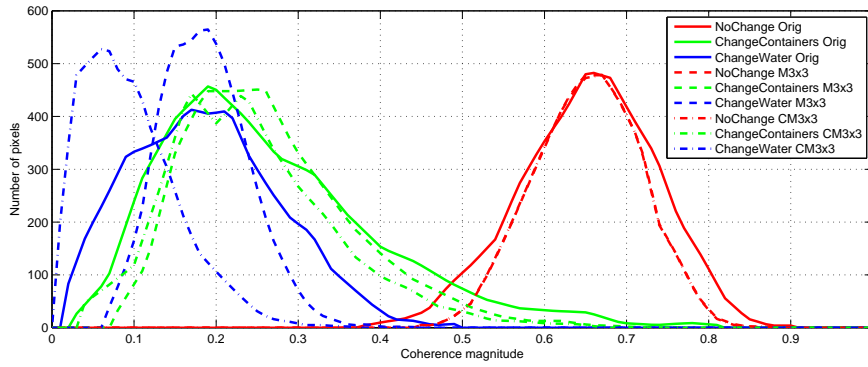


Figure 2. Histograms of the coherence magnitude for the three approaches

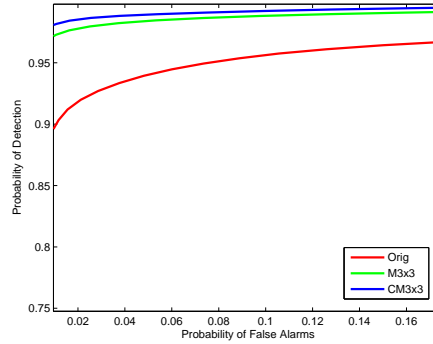


Figure 3. RoC curves for separating the area of "container changes" from the area of "no changes"

### 3.4 Semi-supervised detection and characterization of changes

In order to monitor human activity in the harbor in a semi-automated manner, the different types of changes have to be detected and classified. For a human operator an image as shown in fig. 4(right), showing a composite of the filtered coherence and intensity data, will suffice. However, for long-term semi-automatic monitoring of activities, this image needs to be classified. The developed classification is quite simple and is based on a combination of thresholds on the three features, i.e. the filtered coherence and log-intensity of the Lee-filtered images. The thresholds sub-divide each of the three features into a "low" and "high" value area and are determined from the histograms of the coherence after spatial averaging and the speckle reduced log-intensity data, shown respectively in fig. 2 and fig. 5(right). The actual change detection and characterization is a rule-based set of decisions applied to the thresholded images. Dividing each of the three feature sets into two value regions leads to 8 possible combinations, thus 8 possible classes. Table 3 presents an overview of the properties of the different classes. Classes of interest for change detection and activity monitoring are C2-C4. Classes C1, C5 and C8 contribute to the overall scene understanding. C6 and C7 represent classes in which the coherence is high but the intensity changes between both images. If this situation occurs, it is due to the fact the coherence (or intensity) value supersedes the threshold in a region where it shouldn't (the tails of the histograms). This is mainly due to subsistence of coherence bias even after applying the filter. These two classes represent a very small portion of the image.

Fig.6 shows the classification results obtained by processing two different image pairs. The figure shows that the overall classification of the scene looks quite good. In the sea, outside the port, there is some confusion between the correct class (C1) and class C2. The two rectangles indicate the location of container terminals. It can be seen that the highest density of activity (classes C2, C3 and C4) is located in these two areas. The circle is an example of class C3; it is a ship entering the harbor at the time of acquisition on the 15th of June.

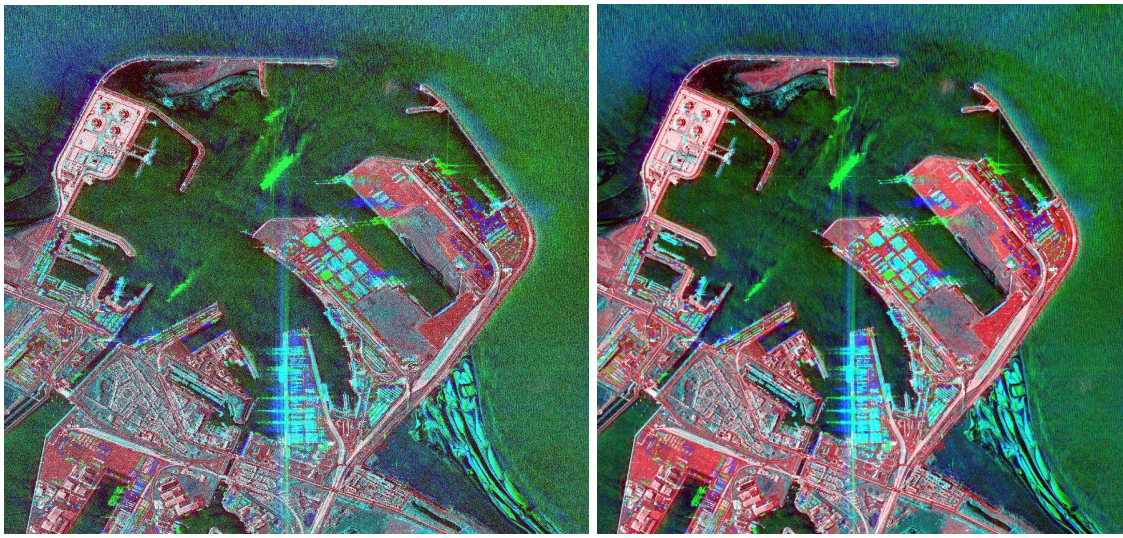


Figure 4. Composite of coherence (red) and intensity data of I1 (green) and I2 (blue) using the original data (left) and the filtered data (right).

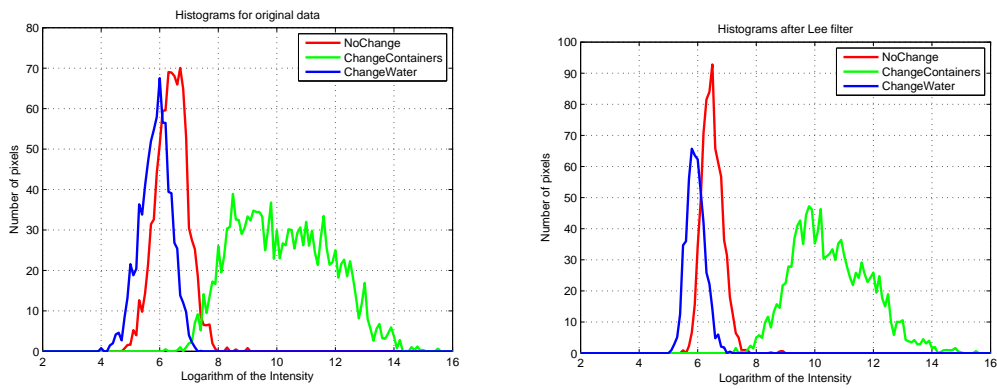


Figure 5. Histograms of the logarithm of the intensity of the three areas in the original data (left) and the data after  $5 \times 5$  Lee filter.

The upper container terminal is mostly classified as C1 in the classification resulting from the combination of the images from the 15th and the 16th of June. In the second dataset, the amount of changes in this area increases. This means that between the 15th and the 19th there were more changes in the container area than between the 15th and the 16th. Fig. 7 shows detailed images of a time sequence of the classification results obtained in this container terminal area. As can be expected, the amount of changes increases with increasing temporal baseline. In a further work the classification between pairs of successive acquisition dates will be determined in order to investigate peaks in activity, but the present results already illustrate the feasibility of such an analysis. The figure also shows the presence of three small ships on the 16th of June, one small ship on the 19th and a larger ship on the 2th of July.

#### 4. SHIP DETECTION WITHIN THE HARBOR

From the classification results discussed above, it is quite easy to detect ships within the harbor. If the ships are different between the two dates corresponding to the acquisition of the interferometric pair, ships should be objects classed as C2 or C3 on the surface of the water. By georeferencing the SAR images and combining them with a digital map of the port, the areas corresponding the water can be easily retrieved. However, as

Class	Features			Interpretation
	Coherence	LogInt(I1)	LogInt(I2)	
C1	L	L	L	Low backscatter: specular surfaces: water, roads, flat roofs, shadows
C2	L	L	H	Change: man-made objects present in I2, not in I1
C3	L	H	L	Change: man-made objects present in I1, not in I2
C4	L	H	H	Change: man-made object present in both images but it changed from I1 to I2
C5	H	L	L	No change and low backscatter: bare soil or low vegetation
C6	H	L	H	Invalid class (mainly due to high coherence bias)
C7	H	H	L	Invalid class (mainly due to high coherence bias)
C8	H	H	H	Strong scatterers present in both scenes: fixed structures (e.g.parts of buildings, railways)

Table 3. Overview of the eight classes resulting from the semi-supervised change detection and classification

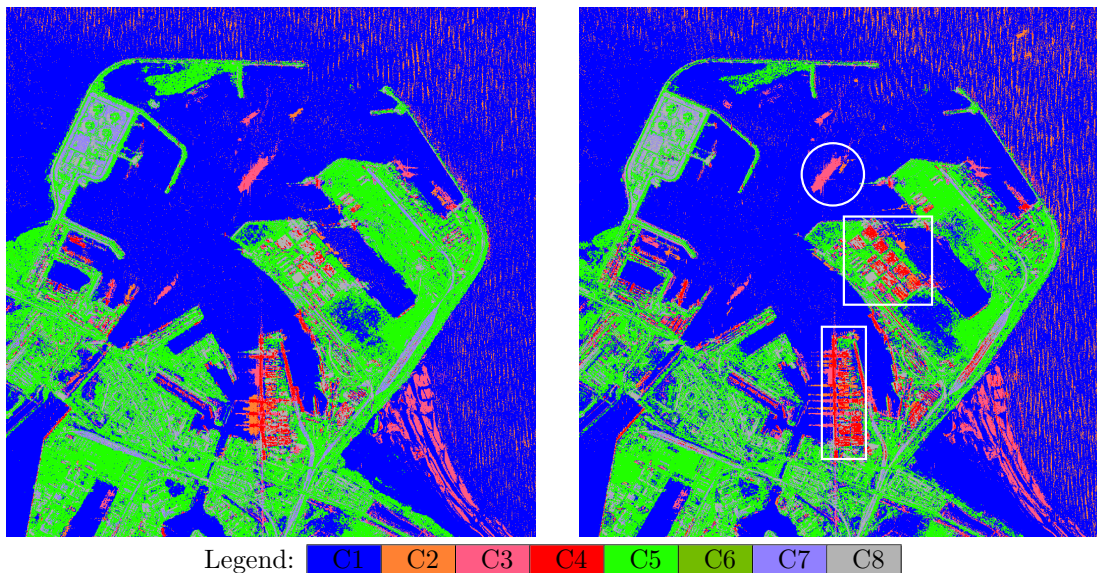


Figure 6. Results of the classification for the image pair 15jun/16jun(left) and 15jun/19jun(right). The rectangle indicate the location of container terminals, the circle is an example of an object classed as C3 (a ship entering on the 15th of June 2011).

an illustration, we used the data from the SAR images for delimiting the water surface directly from the SAR data..

#### 4.1 Delimitation of the water surface

As mentioned above the water should be characterized by a very low coherence in all interferometric pairs and a low intensity in all images. The filtered images are used in order to limit the effect of the bias for low coherences and speckle in the intensity images. The minimum over all interferometric pairs of the filtered coherence images and the minimum over all intensity images is used as input for the water detection. Due to subsistence of some effects of speckle and coherence bias, it was not sufficient to use a simple threshold for delimiting the water. Increasing the size of the filters may reduce this problem, however this will lead to a blurring of the water/land interface. As many of the ships to be detected in the harbor are moored to the quay, this blurring will result in a less correct delimitation of the ships. For that reason a classification method was developed to delimit the water surface based on the application of the small-sized filters discussed above. An approach based on a fuzzy rule-based system<sup>12,13</sup> for combining the different features was applied. Many

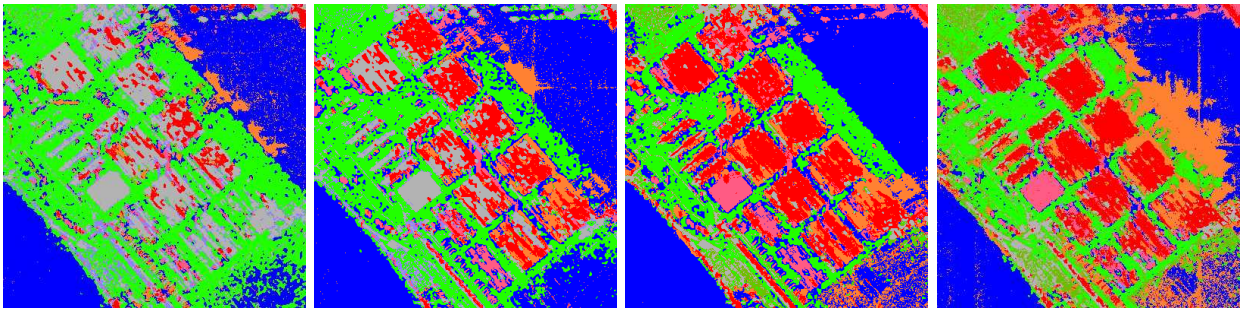


Figure 7. Classification result in the container terminal area between resp. 15jun11/16jun11, 15jun11/19jun11, 15jun11/01jul11 and 15jun11/02jul11.

other types of approaches may be equally effective. The fuzzy system actually was defined for delimiting the land surface. The water is then the complement of its result. Fig. 8 shows the defined membership functions for the detection of the land surface. As there is only one output class for the classification, the fuzzy system is very simple. Fig. 4 shows a graphical representations of the implemented rules.

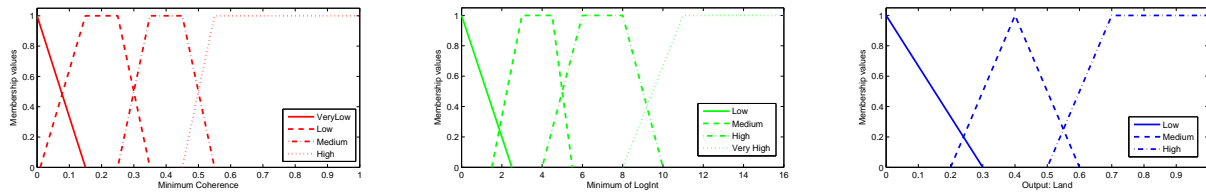


Figure 8. Input membership functions for coherence (left) and intensity (middle) and the output membership function (right) for the detection of the land surface

		Intensity MBF			
		Low	Medium	High	Very High
Coherence MBF	Very low	Low	Low	Medium	High
	Low	Low	Medium	High	High
	Medium	Medium	Medium	High	High
	High	Medium	High	High	High

Table 4. Schematic representation of the rules used in the fuzzy classifier that link the input membership function and the output membership functions.

Although three discrete output membership functions are defined, the fuzzy rule-based system results in an image with a continuous range (between 0 and 1) of values. This image can then be thresholded for obtaining the final result. Prior to this thresholding a spatial regularization is applied based on morphological operators. In particular a sequence of a morphological closing and opening is applied.

## 4.2 Ship detection and validation

Once the water surface is determined, the ships can be detected as objects of class C2 or C3 on the water surface. After georeferencing, these detection results can be compared to the AIS (Automatic Identification of Ships) data that was collected simultaneously with each SAR data acquisition. Fig. 10 shows the georeferenced result of ship detection obtained on the image of the 15th of June and Fig. 11 shows the corresponding AIS data projected on GoogleEarth. There seems to be a slight shift in position of the moving ships between the SAR image and the AIS data. It can be seen that most of the cargo ships in the port have been correctly detected. Only for the "European Trader" only a small part is detected. This is due to the fact that the

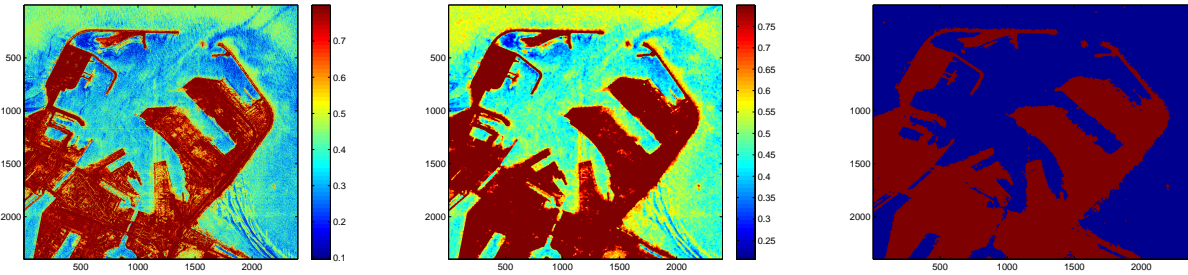


Figure 9. Result of land detection after fuzzy rule-based classification (left) after classification with spatial regularization (middle) and the final thresholded land image (right)

classification was obtained using data from the 15th and 16th of June; the European Trader was present on the 15th, but on the 16th another ship was moored at the same location. Most of the surface common to both ships is therefore classified as C4 and thus discarded for the ship detection.

Near the exit of the harbor a ship is detected that does not appear in the AIS data. Near the Hansa Lubeck, there are also two small detections. These could be two of the three tug boats that are present according to the AIS data (Union Onyx, Union Pearl or Union Coral). Table 5 presents a list of the main ships present in the harbor at the time of the SAR data acquisition as well as their type and dimensions (information retrieved for MarineTraffic.com). Although the results of the ship detection appear good, the approach is pixel-based. This means that ships are sometimes detected as non-connected parts. In further work we will segment the complete ships from the detection results in order to automatically retrieve their size properties.

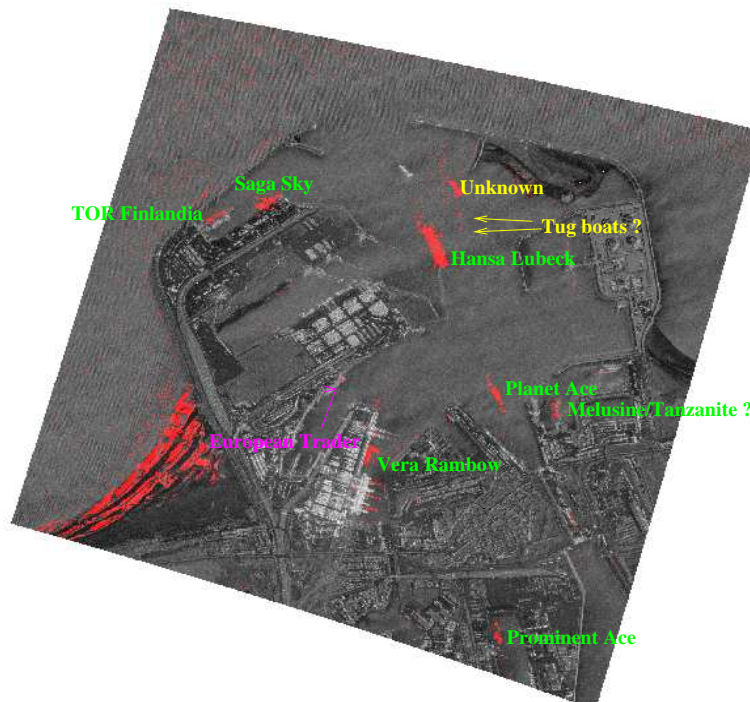


Figure 10. Result of ship detection on the image of June 15th.



Figure 11. AIS data.corresponding to the SAR acquisition of 15th of June 2011

Ship's name	Type	Dimensions
Hansa Lubeck	Reefer	156m × 23m
Vera Rambow	Container ship	169m × 27m
Tanzanite	Inland Tanker	110m × 14m
European Trader	Ro-Ro Cargo	156m × 23m
Planet Ace	Vehicles Carier	188m × 28m
Melusine	Vehicles Carier	162m × 25m
Auto Pride	Vehicles Carier	125m × 18m
Tor Finlandia	Ro-Ro Cargo	162m × 20m
Union Onyx	Tug boat	33m × 11m

Table 5. Overview of type and size of ships present in the harbor on 15th of June 2011 according to the recorded AIS data

## 5. CONCLUSIONS AND FURTHER WORK

In this paper a processing scheme is presented for detection and characterization of changes due to human activities using high-resolution interferometric SAR data. The method is applied to the problem of activity monitoring in a commercial harbor and combines interferometric coherence information and intensity information into a semi-supervised classification. Both coherence and intensity are filtered in order to reduce respectively the coherence bias and the speckle. Because the high interest in detecting small objects in the change detection, filters with a small spatial extend were used. The applied filters facilitate the semi-automatic detection and characterization of changes while keeping a high spatial resolution. The proposed classification retrieves the global structure of the harbor and detects the areas of large activity on land (mainly the container terminals within the harbor). On the other hand the classification also allows to easily detect the presence of ships within the harbor in a semi-automatic fashion. The proposed approach can thus be applied for continuous activity monitoring within the harbor. In further work a larger set of data will be examined for validating the approach further and for detecting peaks of activity.

## 6. ACKNOWLEDGMENTS

The SAR data was obtained through a collaboration within NATO SET145 and kindly provided by e-GEOS in the frame of a demonstration project. We thank the private companies Sarmap and ITTVis for their support in providing a full Sarscape licence (v. 4.8, 2011) included in the latest version of Envi software. The AIS data used in this project was partly provided by the MIK (Maritime Information Junction) at Zeebrugge, by Mr Defruyter of the Belgian Defence and by Dr B. Van den Broek of the Netherlands Organisation for Applied Scientific Research (TNO). Part of the AIS data was extracted from [www.marinetraffic.com](http://www.marinetraffic.com).

## REFERENCES

- [1] Zebker, H. and Villasenor, J., “Decorrelation in interferometric radar echoes,” *IEEE-TGRS* **30**, 950–959 (May 1992).
- [2] Rignot, E. and Zyl, J. V., “Change detection techniques for ers-1 sar data,” *IEEE-TGRS* **31**, 896–906 (Apr 1993).
- [3] Corr, D. and Rodrigues, A., “Coherent change detection of vehicle movements,” in [*Proc. IGARSS’98*], IEEE (1998).
- [4] Preiss, M., Gray, D., and Stacy, N., “Detecting scene changes using synthetic aperture radar interferometry,” *IEEE-TGRS* **44**, 2041–2054 (Aug 2006).
- [5] Sabry, R., “A new coherence formalism for change detection and phenomenology in SAR imagery: A field approach,” *IEEE-GRSL* **6**(3), 458–462 (2009).
- [6] Philips, R., “Clean: A false alarm reduction method for SAR CCD,” in [*Proc. ICASSP*], 1365–1368 (May 2011).
- [7] Johnsen, T., “Coherent change detection in SAR images of harbors with emphasis on indings from container backscatter,” in [*Proc. IGARSS’11*], IEEE, Vancouver, Canada (July 2011).
- [8] “Port of zeebrugge website,” (<http://www.portofzeebrugge.be/>).
- [9] Touzi, R., Lopes, A., Bousquet, P., and Vachon, P., “Coherence estimation for SAR imagery,” *IEEE-TGRS* **37**, 135–149 (January 1999).
- [10] Bouaraba, A., Borghys, D., Belhadj-Aissa, A., Acheroy, M., Milisavljevic, N., and Closson, D., “Coherent change detection performance using high-resolution SAR images,” *Progress in Electromagnetic Research* (Submitted 2012).
- [11] Lee, J., “Digital image enhancement and noise filtering by use of local statistics,” *IEEE-PAMI* **2**, 165–168 (Mar 1980).
- [12] Zadeh, L., “Fuzzy logic and the calculi of fuzzy rules and fuzzy graphs,” *Multiple-Valued Logic* **1**, 1–38 (1996).
- [13] *Fuzzy Logic Toolbox for use with MATLAB: User’s Guide*.